

Coriolis-Zeeman effect in rotating photonic crystal

D.L. Boiko*

*École Polytechnique Fédérale de Lausanne,
Quantum Architecture group, 1015, Lausanne, Switzerland*

(Dated: February 6, 2020)

Abstract

Rotation-induced splitting of the otherwise degenerate photonic bands is predicted for a two-dimensional photonic crystal made of evanescently coupled microcavities. The symmetry-broken energy splitting is similar to the Zeeman splitting of atomic levels or electron's (hole's) magnetic moment sublevels in an external magnetic field. The orbital motion of photons in periodic photonic lattice of microcavities is shown to enhance significantly such Coriolis-Zeeman splitting as compared to a solitary microcavity [D.L. Boiko, *Optics Express* **2**, 397 (1998)]. The equation of motion suggests that nonstationary rotation induces quantum transitions between photonic states and, furthermore, that such transitions will serve as a source of nonstationary gravitational field.

PACS numbers: 42.70.Qs, 71.70.Ej, 03.65.Pm, 03.30.+p.

The Sagnac effect in a rotating ring cavity, known also as the Coriolis-Zeeman effect for photons, emerges as a frequency splitting of counterpropagating waves¹. Thus, for a ring cavity of M wavelengths optical path, the modal shift is $M\Omega$. Nowadays, the effect is used in commercial He-Ne ring laser gyros of large ($M\sim 10^6$) cavity size. Significant efforts were made towards designing miniature-sized solid-state devices based on a high optical gain medium². Theoretical investigation has been carried out about the impact of rotation on the whispering gallery modes of a microdisc microstructure³. Here, the frequency splitting scales with the closed optical path length, while the field polarization is either not relevant or assumed to be parallel to the rotation axis Ω .

On the other hand, the Coriolis-Zeeman effect in a cylindrical microwave resonator rotating along the symmetry axis⁴ or in an optical Fabry-Pérot cavity rotating in the mirror plane is, at first sight, independent of the cavity size⁵. The frequency shift $(S+M)\Omega$ of polarization and transversal modes is set by the spin (± 1) and the azimuth mode index M . However, the higher is the mode index M , the larger is the size of the cavity that will support such mode. By virtue of the complexity of the mode discrimination at high M and because of the small frequency splitting of the polarization modes, this effect has not yet been verified in experimental measurements.

In this Letter, I consider the Coriolis-Zeeman effect in coupled microcavities arranged in a periodic two-dimensional (2D) lattice in the plane of rotation [Fig.1(a)]. On example of a square-symmetry lattice, the possibility of enhanced Coriolis-Zeeman splitting, corresponding to $M\sim 1000$, is predicted for the *low-order* photonic modes⁶. It is caused by the photon's orbital motion extended over the large number of lattice cells. The equation of motion, which is similar to the Hamiltonian for electrons and holes in magnetic field, suggests that nonstationary rotation induces quantum transitions between photonic states and, vice versa, that such transitions will generate a nonstationary gravitational field.

Arrays of evanescently coupled microcavities belong to a particular sub-class of 2D photonic crystal (PhC) structures encompassing photonic crystal fibers and arrays of microcavities. Matrices of vertical cavity surface emitting lasers (VCSELs) are an example of such 2D photonic crystals⁷. In such structures, only a small transversal component \mathbf{k}_\perp of the propagation vector \mathbf{k} undergoes Bragg reflections in the plane of periodic lattice [Fig.1(a)]. The structures employ lattices of periods significantly exceeding the optical wavelength. They are typically realized by the mirror reflectivity patterning in a broad-area microcavity.

As a model system for such PhC structures, a Fabry-Pérot cavity with patterned mirror reflectivity is considered here. The cavity length is one wavelength, $l_z=\lambda/n$ with n being the refractive index in the cavity. The reflectivity $R_1(x, y)$ of the one cavity mirror (*e.g.*, of the top mirror) is modulated in two directions parallel to its plan. The reflectivity pattern $R_1=\exp i\varphi(x, y)$ consists of pixels with the relative phase shift $\varphi(x, y)=\Delta\varphi$ separated by a grid of $\varphi(x, y)=0$. The mirror is thus perfectly reflecting ($|R_1|=1$) and the phase modulation pattern $\varphi(x, y)$ defines the structure of the cavity modes. The period of the reflectivity pattern Λ is of a few micron pitch ($\Lambda\gg l_z$). The pattern is characterized by a fill factor FF that is the ratio between the area of the pixel and that of the unit cell. Like in typical VCSEL arrays, the phase contrast of reflectivity pattern is small ($|\Delta\varphi|\lesssim 10^{-2}$). The second mirror of uniform reflectivity ($R_2=1$) has no impact on the cavity modes.

The analysis is carried out here using an equivalent, unfolded cavity representation⁸. Multiple reflections at the cavity mirrors effectively translate the cavity into a structure that is periodic along the cavity axis (the z -axis). The unfolded PhC is thus three-dimensional and it can be analyzed in terms of a modal expansion on orthogonal plane waves (OPWs). The Coriolis-Zeeman effect in such photonic crystal is considered here using a frame of reference, which rotates together with the crystal. Such noninertial rest frame is characterized by a metric tensor g_{ik} , the off-diagonal space-time components $g_{0\alpha}$ of which are dependent on the angular rotation speed Ω ⁹. However, in the unfolded-cavity representation, g_{ik} differs from the diagonal Minkowski tensor, even in the absence of rotation. Thus $g_{0\alpha}\neq 0$ at the subsequent mirror reflections since the reflection operator $\hat{\sigma}=\hat{I}\hat{C}_2$ includes rotation by π (about the z axis) followed by coordinate inversion [Fig.1(a)]. Due to the patterned mirror reflectivity, the equivalent unfolded PhC is of periodically varying "noninertiality" in the xy plane⁸. In the approximation of the first-order terms $\Omega r/c$ and $\Delta\varphi$, the metric tensor g_{ik} has the following nonzero components:

$$\begin{aligned} g_{00} &= -g_{11}=-g_{22}=-g_{33}=1, \\ g_{0\alpha} &= -\frac{1}{c}e_{\alpha\beta\gamma}\Omega^\beta x^\gamma -\delta_{\alpha 3}\frac{c}{\omega}\varphi(x^1, x^2)\sum_j\delta(x^3-2jl_z), \end{aligned} \quad (1)$$

where $g_{0\alpha}=g_{\alpha 0}$ ($\alpha = 1, 2, 3$), the space-time coordinates are indexed according to the intervals $dx^0=cdt$, $dx^1=dx$, $dx^2=dy$ and $dx^3=dz$; twice repeated Greek indexes indicate summation. The first term in $g_{0\alpha}$ accounts for rotation of the coordinate system¹. The second term accounts for the multiple cavity roundtrips along the z -axis and reflections at the cavity

mirrors. The z -period of the unfolded crystal is thus $2l_z$. The metric tensor (1) is validated by inspecting the system Hamiltonian [Eq.(7)] for the case of $\varphi=0$ (rotating FP cavity⁵) or $\Omega=0$ (PhC in an inertia frame⁸).

In the approximation (1), the coordinate space is Euclidean, with the metric tensor $\gamma_{\alpha\beta} = -g_{\alpha\beta} + g_{0\alpha}g_{0\beta}/g_{00}$ being the Kronecker delta $\delta_{\alpha\beta}$. Proceeding in a standard manner⁹, the covariant Maxwell's equations with metric (1) are converted to the usual form in terms of noncovariant field vectors \mathbf{B} , \mathbf{H} , \mathbf{D} and \mathbf{E} that assume the constitutive equations

$$\begin{aligned} \mathbf{D} &= \varepsilon \mathbf{E} + \mathbf{H} \times \mathbf{g}, & \mathbf{B} &= \mu \mathbf{H} + \mathbf{g} \times \mathbf{E}, \\ \mathbf{g} &= \frac{\boldsymbol{\Omega} \times \mathbf{r}}{c} + \hat{\mathbf{z}} \frac{c}{\omega} \varphi(\mathbf{r}_\perp) \sum_j \delta(z - 2jl_z), \end{aligned} \quad (2)$$

where $\hat{\mathbf{z}}$ is the unit vector along z -axis direction and the components of the vector \mathbf{g} are $g_\alpha = -g_{0\alpha}/g_{00}$.

Maxwell' equations in photonic crystal (2) are solved here by separating fast oscillations in the z -axis direction and slow lateral field oscillations in the xy plane:

$$\begin{bmatrix} E_\alpha \\ H_\gamma \end{bmatrix} = e^{ik_z z - i\omega t} \frac{1 + \eta(z)}{\sqrt{2\pi}} \begin{bmatrix} Z^{\frac{1}{2}} \hat{\mathcal{E}}_{\alpha\beta} \\ Z^{-\frac{1}{2}} e_{3\beta\alpha} \hat{\mathcal{E}}_{\gamma\alpha} \end{bmatrix} \boldsymbol{\psi}_\beta(\mathbf{r}_\perp), \quad (3)$$

where $n = \sqrt{\varepsilon\mu}$ and $Z = \sqrt{\mu/\varepsilon}$ are the refractive index and impedance in the cavity. The gauge transformation is introduced here through the operator

$$\begin{aligned} \hat{\mathcal{E}}_{\alpha\beta} &= \delta_{\alpha\beta} \left(1 - \frac{1}{4k_z^2} \frac{\partial^2}{\partial x_\gamma \partial x_\gamma} \right) + \frac{1}{2k_z^2} \frac{\partial^2}{\partial x_\alpha \partial x_\beta} \\ &+ i \frac{\delta_{\alpha 3}}{k_z} \frac{\partial}{\partial x_\beta} + \frac{\Omega}{nc} e_{3\gamma\beta} \left(\delta_{\alpha 3} x_\gamma - i \frac{x_\alpha}{k_z} \frac{\partial}{\partial x_\gamma} \right), \end{aligned} \quad (4)$$

where the terms $\sim k_\perp^2/k_z^2$ are taken into account. Such separation of variables is valid in conditions of the paraxial approximation ($\frac{1}{k_z^2} \left| \frac{\partial^2 \psi_\alpha}{\partial x_\beta \partial x_\gamma} \right| \ll \frac{1}{k_z} \left| \frac{\partial \psi_\alpha}{\partial x_\beta} \right| \ll 1$) and of the low contrast of reflectivity pattern ($|\Delta\varphi| \ll 1$). The two-component vector $\boldsymbol{\psi}(\mathbf{r}_\perp) = \begin{pmatrix} \psi_x \\ \psi_y \end{pmatrix}$ in the x - y plane is a slowly-varying function of coordinates. It defines the spatial patterns of the six electromagnetic field components (3) and it is considered here as the photonic state wave function. Its squared modulus $|\boldsymbol{\psi}(\mathbf{r}_\perp)|^2$ yields the intensity pattern of the main polarization component in (3). For $\Omega=0$, Eqs.(3)-(4) are in agreement with the results obtained for the Gaussian beam¹⁰.

In photonic crystals, the wave function $\boldsymbol{\psi}(\mathbf{r}_\perp)$ is a Bloch wave propagating in the xy plane⁸,

$$\boldsymbol{\psi}_{q\mathbf{k}_\perp} = e^{i\mathbf{k}_\perp \cdot \mathbf{r}_\perp} \mathbf{u}_{q\mathbf{k}_\perp}(\mathbf{r}_\perp), \quad (5)$$

where $\frac{4\pi^2}{\Lambda^2} \int_{\text{cell}} \mathbf{u}_{q'\mathbf{k}_\perp}^* \mathbf{u}_{q\mathbf{k}_\perp} d^2\mathbf{r}_\perp = \delta_{q'q}$ ¹². The longitudinal part in (3) [the term $e^{ik_z z \frac{1+\eta_{q\mathbf{k}}(z)}{\sqrt{2\pi}}}$] is also a Bloch function. Within the z -period of the lattice, it has a small modulation depth $\langle |\eta_{q\mathbf{k}}| \rangle_{2l_z} = \frac{1}{2l_z} \int_{-l_z}^{l_z} |\eta_{q\mathbf{k}}| dz \sim \Delta\varphi$, which is set by an effective phase shift $\alpha_{q\mathbf{k}}$ at each reflection of the patterned mirror. The general form of such periodic function $\eta_{q\mathbf{k}}$ is

$$1+\eta_{q\mathbf{k}} = \exp \left\{ i\alpha_{q\mathbf{k}} \sum_j \left[\theta(z-2jl_z) - \frac{1}{2} \right] - \frac{iz\alpha_{q\mathbf{k}}}{2l_z} \right\} \quad (6)$$

where $\theta(z) = \int_{-\infty}^z \delta(\zeta) d\zeta$ is the unit step function. Note that $\eta_{q\mathbf{k}}(z)$ is the odd function and $\langle \partial\eta_{q\mathbf{k}}/\partial z \rangle_{2l_z} \simeq 0$ by virtue of the small contrast of the reflectivity pattern.

By operating with $e_{3\beta\alpha} \hat{\mathcal{E}}_{\gamma\alpha}^{-1}$ and $\hat{\mathcal{E}}_{\alpha\beta}^{-1}$ [from (4)] on Maxwell' equations for the curl of \mathbf{E} and \mathbf{H} , substituting the gauge (3) and averaging over the z -period of the lattice, the Maxwell' equations are converted into the same form of a Hamiltonian eigenproblem with respect to the photonic state wave function $\boldsymbol{\psi}_{q\mathbf{k}}(\mathbf{r}_\perp)$

$$\left(\frac{m_0 c^2}{n^2} + \frac{\hat{\mathbf{p}}_\perp^2}{2m_0} - \frac{c\hbar}{2nl_z} \varphi(\mathbf{r}_\perp) \right) \boldsymbol{\psi}_{q\mathbf{k}} - \frac{\Omega}{n^2} \left(\mathbf{r}_\perp \times \hat{\mathbf{p}}_\perp + \hbar \hat{S}_z \right) \boldsymbol{\psi}_{q\mathbf{k}} = \hbar\omega_{q\mathbf{k}} \boldsymbol{\psi}_{q\mathbf{k}}, \quad (7)$$

where $m_0 = n\hbar k_z / c$ and $\hat{S}_z = i\hat{\mathbf{z}} \times$ is the spin operator that reads $(\hat{S}_z)_{\alpha\beta} = ie_{\alpha 3\beta} = \begin{pmatrix} 0 & -i \\ i & 0 \end{pmatrix}$ in the basis of the two-component vector functions $\boldsymbol{\psi} = \begin{pmatrix} \psi_x \\ \psi_y \end{pmatrix}$. Solutions of Eq.(7) define the slowly-varying components of photonic modes (3). The difference between the exact equation for $(1+\eta_{q\mathbf{k}})\boldsymbol{\psi}_{q\mathbf{k}}$ and its z -period average [Eq.(7)] yields the equation for the periodic part of the fast longitudinal component:

$$\frac{\partial\eta_{q\mathbf{k}}}{\partial z} = i\alpha_{q\mathbf{k}} (1 + \eta_{q\mathbf{k}}) \left[\sum_j \delta(z - 2jl_z) - \frac{1}{2l_z} \right] \quad (8)$$

where $\alpha_{q\mathbf{k}} = \langle \boldsymbol{\psi}_{q\mathbf{k}} | \varphi | \boldsymbol{\psi}_{q\mathbf{k}} \rangle$. The solution of (8) is given by (6) provided that the eigen functions $\boldsymbol{\psi}_{q\mathbf{k}}$ of the Hamiltonian (7) are known.

In (7), the first term is due to the paraxial propagation along the z axis. The second and third terms are the in-plane kinetic energy and the periodic crystal potential, respectively.

The last term in (7) is a perturbation induced by the Coriolis force. For $\varphi=0$ and $\Omega=0$, within the accuracy of the time variable, Eq.(7) is just the paraxial wave equation. For $\varphi=0$, Eq.(7) yields the effective refractive index $\frac{c}{\omega}(k_z + \frac{k_\perp^2}{2k_z})$ of a circularly-polarized paraxial wave

$$n_{\text{eff}} = n + \mathbf{g}\boldsymbol{\tau} \pm \frac{\Omega\boldsymbol{\tau}}{\omega n}, \quad (9)$$

where $\boldsymbol{\tau} = \frac{\mathbf{k}}{k}$ defines the propagation direction, $+/-$ sign is for the left/right handed polarization. Eq.(9) agrees with previously reported expressions for the axial nonreciprocity¹ (second term) and circular birefringence⁵ (third term) induced by the Coriolis force for photons. Finally, the unperturbed ($\Omega=0$) Hamiltonian has been verified by experimental measurements in VCSEL array PhC heterostructures¹¹. These justify the approximation (7) of the Hamiltonian.

Analytical similarities between the effective single-electron Hamiltonian in a semiconductor subjected to an external magnetic field and Eq.(7) allow the correspondence between the periodic crystal potential V and phase pattern φ ($V \rightarrow -\frac{c\hbar}{2nL}\varphi$), and the vector potentials $\mathbf{A} = \frac{1}{2}\mathbf{H} \times \mathbf{r}$ and $\mathbf{g}_\perp = \frac{1}{c}\boldsymbol{\Omega} \times \mathbf{r}$ ($\frac{e}{c}\mathbf{A} \rightarrow \frac{m_0 c}{n^2}\mathbf{g}_\perp$). Photons in photonic crystal subjected to a nonpermanent gravitainoal field exhibit thus a similar behaviour with electrons (holes) in a magnetic field. Accordingly, the impact of rotation on the envelope function and periodic part of the photonic Bloch wave (5) is different. Like in the case of electrons,¹² the components of velocity operator $\hat{\mathbf{v}}_\perp = \frac{1}{i\hbar}[\mathbf{r}_\perp, \hat{H}]$ do not commute ($[\hat{v}_x, \hat{v}_y] = -\frac{2i\hbar}{m_0 n^2}\Omega_z$, where $\hat{\mathbf{v}}_\perp = \frac{\hat{\mathbf{p}}_\perp}{m_0} - \frac{\boldsymbol{\Omega} \times \mathbf{r}_\perp}{n^2}$). However, the second-order terms $\sim \frac{\Omega^2 r^2}{c^2}$ in the Hamiltonian (7) [and, respectively, in (1)] are needed to define whether the Landau-like quantization is possible for photonic envelope wave functions. In the rest of the Letter, the impact of rotation on the periodic part of Bloch functions is examined in details on example of a square-lattice PhC.

Fig.1(b) shows the typical band structure of a square-lattice PhC, which is calculated along the high symmetry lines Δ - Z - T in the Brillouin zone (BZ), using the OPW expansion in unperturbed ($\Omega=0$) Hamiltonian. By virtue of the square lattice symmetry, all states are degenerate by the photon's spin (*e.g.*, the doubly degenerate states \mathbf{T}_5 or \mathbf{T}'_5). Angular rotation removes the degeneracy of such states and splits their energies on $2\frac{\hbar\Omega}{n^2}$ [Fig.2(a), top panel]. However, there are states, like the degenerate states \mathbf{T}_1 , \mathbf{T}_2 , \mathbf{T}_3 and \mathbf{T}_4 , of the four-fold degeneracy, which is caused by the orbital symmetry of the Bloch functions. For such states, there is an important angular momentum contribution $\frac{1}{n^2}\hbar\Omega_z\hat{L}_z$ to the energy shift.

The Coriolis-Zeeman splitting of these states is analyzed here using the first-order $\mathbf{k}\mathbf{p}$ expansion in the T point [$\mathbf{k} = (\frac{\pi}{\Lambda}, \frac{\pi}{\Lambda}, k_z)$] of the BZ. The expansion basis is deduced from the empty lattice test. Four scalar plane waves $\exp(\pm\frac{\pi x}{\Lambda} \pm \frac{\pi y}{\Lambda})$, which form the first photonic band of empty lattice, originate from the nearest equivalent T points of reciprocal lattice and provide representation that is reducible under the C_{4v} point group (the symmetry group of \mathbf{k}). Their symmetrized combinations of T_1 , T_4 and T_5 representations are indicated in the second column of Table I with the capitals letters corresponding to the main term of Taylor expansion on parameter $\frac{|\mathbf{r}_\perp|}{\Lambda}$ (e.g., $|S\rangle = \frac{1}{\pi} \cos \frac{\pi x}{\Lambda} \cos \frac{\pi y}{\Lambda}$, $|iX\rangle = \frac{i}{\pi} \sin \frac{\pi x}{\Lambda} \cos \frac{\pi y}{\Lambda}$). The photon's spin transforms as the two-dimensional representation T_5 . Therefore, a reduction of the direct product $T_i \otimes T_5$ results in the eight symmetry adapted photonic harmonics of \mathbf{T}_1 - \mathbf{T}_5 and \mathbf{T}'_5 representations that constitute a suitable $\mathbf{k}\mathbf{p}$ -expansion basis in the low-order photonic bands. These states are well separated energetically from the other states in the T point [Fig.1(b)].

For a general state $|\psi_{q\mathbf{k}}\rangle = e^{i\mathbf{k}_\perp \cdot \mathbf{r}_\perp} \sum_i c_i |\mathbf{T}_i\rangle$ at \mathbf{k}_\perp measured from the T point of the BZ, the 8x8 $\mathbf{k}\mathbf{p}$ Hamiltonian for the coefficients c_i is of the block-diagonal form

$$\hat{H} = \begin{bmatrix} \hat{H}_0 + \hat{H}_{\mathbf{k}\mathbf{p}} + \hat{H}_\Omega + \frac{\hbar^2 k^2}{2m_0} & 0 \\ 0 & \hat{H}_0 + \hat{H}_{\mathbf{k}\mathbf{p}}^* - \hat{H}_\Omega + \frac{\hbar^2 k^2}{2m_0} \end{bmatrix} \quad (10)$$

where

$$\hat{H}_0 = \begin{bmatrix} \hbar\omega_{T'_5} & 0 & 0 & 0 \\ 0 & \hbar\omega_{T_1} & 0 & 0 \\ 0 & 0 & \hbar\omega_{T_1} & 0 \\ 0 & 0 & 0 & \hbar\omega_{T_5} \end{bmatrix}, \quad \hat{H}_{\mathbf{k}\mathbf{p}} = \frac{\hbar P}{m_0} \begin{bmatrix} 0 & k_- & k_+ & 0 \\ k_+ & 0 & 0 & k_- \\ k_- & 0 & 0 & -k_+ \\ 0 & k_+ & -k_- & 0 \end{bmatrix},$$

$$\hat{H}_\Omega = -\frac{\hbar\Omega}{n^2} \begin{bmatrix} 1 & -M_- \frac{\hbar k_-}{2P} & M_- \frac{\hbar k_+}{2P} & 0 \\ -M_- \frac{\hbar k_+}{2P} & -M+1 & 0 & -M_+ \frac{\hbar k_-}{2P} \\ M_- \frac{\hbar k_-}{2P} & 0 & M+1 & -M_+ \frac{\hbar k_+}{2P} \\ 0 & -M_+ \frac{\hbar k_+}{2P} & -M_+ \frac{\hbar k_-}{2P} & 1 \end{bmatrix}$$

in the basis of functions $\frac{1}{\sqrt{2}}(\mathbf{T}'_{5x} \pm i\mathbf{T}'_{5y})$, $\frac{\mp i}{\sqrt{2}}(\mathbf{T}_1 \mp i\mathbf{T}_2)$, $\frac{\pm i}{\sqrt{2}}(\mathbf{T}_3 \pm i\mathbf{T}_4)$, $\frac{\mp i}{\sqrt{2}}(\mathbf{T}_{5x} \pm i\mathbf{T}_{5y})$ ¹³. The upper (lower) sign refers to the top (bottom) 4x4 block. In (10), $k_\pm = k_x \pm ik_y$, $P = \frac{1}{\sqrt{2}}\langle S | -i\hbar \frac{\partial}{\partial x} | iX \rangle = \frac{\hbar\pi}{\sqrt{2}\Lambda}$ is the interband matrix element of $\hat{\mathbf{p}}$ that defines the band mixing. The eigen solutions of (10) are plotted in Fig.1(b). Good agreement with the band structure calculated from Eq.(7) justifies the first-order $\mathbf{k}\mathbf{p}$ approximation (10) of the system Hamiltonian.

The matrix \hat{H}_Ω in (10) is a perturbation induced by rotation. It accounts for the Coriolis-Zeeman energy shift, which is of the opposite sign for the left (upper 4x4 block) and right

(lower block) handed polarization states of the same orbital symmetry. The rotation lifts degeneracy between such spin states, producing the frequency splitting $\Delta\omega_S = 2\frac{\Omega}{n^2}$, as indicated in Fig.2(a) [top panel] on example of the $\hat{\mathbf{T}}_5$ ($\hat{\mathbf{T}}'_5$) states. In (10), the parameter $M = M_+ + M_-$ accounts for the orbital part of wave functions. The orbital contribution $\Delta\omega_L = 2\frac{M\Omega}{n^2}$ to the Coriolis-Zeeman energy shift $\pm\frac{1}{2}\hbar\Delta\omega_L \pm\frac{1}{2}\hbar\Delta\omega_S$ in the \mathbf{T}_1 - \mathbf{T}_4 states is shown in the bottom panel of Fig.2(a) ($\Delta\omega_S$ is not visible at the scale of $\Delta\omega_L$). The energy shift $\pm\frac{1}{2}\hbar\Delta\omega_L$ [the term $-\frac{\Omega}{n^2}\mathbf{r}\times\hat{\mathbf{p}}$ in Eq.(7)] is evaluated here using the relationship $\mathbf{r}_{mn} = \frac{i\hbar}{m_0} \frac{\mathbf{p}_{mn}}{E_n - E_m}$. Note that the procedure to evaluate the matrix elements of $\hbar\hat{L}_z = \mathbf{r}_\perp \times \hat{\mathbf{p}}_\perp$ in free space¹⁴ and in periodic lattices¹⁵ is different. Here, the f -sum rule $\frac{1}{m_{\alpha\beta}} = \frac{\delta_{\alpha\beta}}{m_0} + \frac{2}{m_0^2} \sum_n \frac{p_{mn}^\alpha p_{nm}^\beta}{E_n - E_m}$ ¹² implies that $M_\pm = \mp\frac{1}{2}(\frac{m_0}{m_{T_5, T'_5}} - 1)$ and

$$\Delta\omega_L = \frac{\hat{\mathbf{z}}\Omega}{n^2} \left[\frac{m_0}{m_{T'_5}} - \frac{m_0}{m_{T_5}} \right], \quad \Delta\omega_S = 2\frac{\hat{\mathbf{z}}\Omega}{n^2}. \quad (11)$$

For an array of square pixels defining the microcavities, $M_\pm = \frac{2nl_z P^2}{\hbar m_0 c F F \Delta\varphi} \left[\frac{\sin\pi\sqrt{FF}}{\pi\sqrt{FF}} (1 \pm \frac{\sin\pi\sqrt{FF}}{\pi\sqrt{FF}}) \right]^{-1}$. It follows that reducing the effective mass (via the lattice pitch Λ , fill factor FF and contrast $\Delta\varphi$), one can enhance the Coriolis-Zeeman splitting and achieve M of more than 10^3 . [Fig.2(b) shows the ratio $\frac{\Delta\omega_L}{\Omega} = \frac{2M}{n^2}$, left axis]. The enhancement is caused by the weak localization of photonic wave functions to the lattice sites. The intraband matrix element $\langle q\mathbf{k} | \mathbf{r}^2 | q\mathbf{k} \rangle = \frac{\hbar^2(M_-^2 + M_+^2)}{2P^2}$ in the \mathbf{T}_1 - \mathbf{T}_4 bands indicates that the wave functions (and, hence, the photon's orbital motion) spread over a large PhC crystal domain [Fig.2(b) right axis], such that $\frac{\Delta\omega_L}{\Omega} = \frac{2\pi\sqrt{2\langle \mathbf{r}_\perp^2 \rangle}}{n^2\Lambda} [1 + \text{sinc}^2\pi\sqrt{FF}]^{-1}$. In the bands of \mathbf{T}_5 symmetry, the intraband matrix elements of \mathbf{r}^2 are nonzero as well, however, the orbital contribution to the Coriolis-Zeeman energy vanishes, in accordance with the group theory selection rules. With present experimental techniques, the predicted frequency splitting [Fig.2(a)] can be validated by direct measurements.

The analogy between Eq.(7) and electron's (hole's) magnetic moment Hamiltonian suggests that a nonstationary field $\mathbf{g}(t)$ will stimulate transitions between the photonic states, and that such transitions will serve as a source for nonpermanent gravitational field $\mathbf{g}(t)$.

The author is grateful to Eli Kapon, Marc-André Dupertuis and Edoardo Charbon, as well as to the Fonds National Suisse de la Recherche Scientifique.

* Electronic address: dmitri.boiko@epfl.ch

- ¹ C.V. Heer, Phys. Rev. **134**, A799 (1964); Proc. of the Third International Conference on Quantum Electronics (Columbia University Press, New York) 1305 (1963); A.M. Khromykh, Zh. Eksp. Teor. Fiz. **50**, 281 (1966); E.J. Post, Rev. Mod. Phys. **39**, 475 (1967).
- ² D.L. Boiko *et al.*, Lazernye Novosti - Laser News **2**, 11 (1997); Quantum Electronics **28**, 355 (1998); H. Cao *et al.*, Appl. Phys. Lett. **86**, 041101 (2005).
- ³ S. Nojima, J. Phys. Soc. Jpn. **73**, 792 (2004).
- ⁴ A.M. Belonogov, Russian Physics Journal **12**, 672 (1969); Sov. Phys. Tech. Phys.-USSR **14**, 883 (1970).
- ⁵ D.L. Boiko, Optics Express **2**, 397 (1998).
- ⁶ A first account of these results was presented at the NFO-9 conference [D. L. Boiko, 9-th International Conference on Near-field Optics, Nanophotonics and Related Techniques, Lausanne, Switzerland, 10-15 September 2006, post-deadline paper ThP-78].
- ⁷ M. Orenstein *et al.*, Appl. Phys. Lett. **60**, 1535 (1992); P.L. Gourley *et al.*, Appl. Phys. Lett. **58**, 890 (1991).
- ⁸ D.L. Boiko *et al.*, Optics Express **12**, 2597 (2004).
- ⁹ L.D. Landau and E.M. Livshits, *The Classical Theory of Fields* (Nauka, Moscow 1988).
- ¹⁰ W.L. Erikson and S. Singh, Phys. Rev. E **49**, 5778 (1994).
- ¹¹ G. Guerrero *et al.*, Optics Express **12**, 4922 (2004).
- ¹² J. M. Luttinger, Phys. Rev. **102**, 1030 (1956); J. M. Luttinger and W. Kohn, Phys. Rev. **97**, 869 (1955).
- ¹³ The wave functions are $\frac{1}{\sqrt{2}}XY(\hat{x}\pm i\hat{y})$, $\pm\frac{1}{2}(X\mp iY)(\hat{x}\pm i\hat{y})$, $\mp\frac{1}{2}(X\pm iY)(\hat{x}\pm i\hat{y})$, $\mp\frac{i}{\sqrt{2}}S(\hat{x}\pm i\hat{y})$.
- ¹⁴ A.T. O'Neil, I. MacVicar, L. Allen, M.J. Padgett, Phys. Rev. Lett. **88**, 053601 (2002); J. Courtial *et al.*, Optics Express **14**, 938 (2006).
- ¹⁵ G.L. Bir and G.E. Pikus, *Symmetry and strain-induced effects in semiconductors* (Nauka, Moscow 1972)

Figures

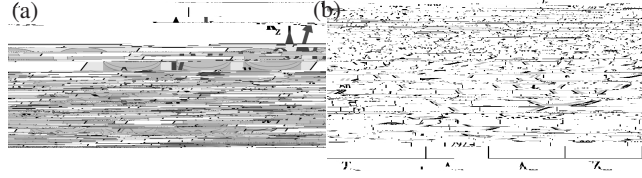


FIG. 1: (a): Schematic of the array of coupled microcavities. (b): Band structure of square-lattice PhC calculated from (7) [black curves] and using 8x8 $\mathbf{k}\cdot\mathbf{p}$ approximation (10) [gray curves]. The inset shows the BZ and location of the high-symmetry triangle ΔZT . The parameters are $\lambda=960nm$, $n=3.53$, $\Lambda=4\mu m$, $FF=0.65$ and $\Delta\varphi=0.02$.

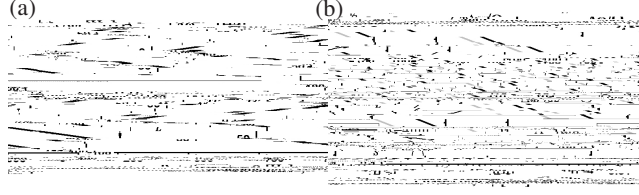


FIG. 2: (a): Coriolis-Zeeman splitting of the \mathbf{T}_5 (\mathbf{T}'_5) (top panel) and \mathbf{T}_1 - \mathbf{T}_4 (bottom panel) bands as a function of rotation rate Ω . $\Lambda = 4\mu m$ and $\Delta\varphi = 10^{-4}$. (b): Relative splitting $\frac{\Delta\omega_{L,S}}{\Omega}$ (left axis) and matrix element $\langle \mathbf{T}_1 | \mathbf{r}^2 | \mathbf{T}_1 \rangle^{\frac{1}{2}}$ (right axis) as a function of the lattice contrast $\Delta\varphi$. The lattice constant Λ is 4 (black curves) and $6\mu m$ (gray curves), $n = 3.53$. Other parameters are given in the caption of Fig.1.

Tables

TABLE I: Basis functions (scalars) and photonic harmonics (vectors) of irreducible representations of the group of \mathbf{k} at the T point of the BZ (C_{4v} point group)

T_i		$T_i \times T_5$	
T_1	S	\mathbf{T}_5	$S\hat{\mathbf{x}}, S\hat{\mathbf{y}}$
T_2	$XY(X^2 - Y^2)$	\mathbf{T}_5''	$XY(X^2 - Y^2)\hat{\mathbf{x}}, XY(X^2 - Y^2)\hat{\mathbf{y}}$
T_3	$X^2 - Y^2$	\mathbf{T}_5'''	$(X^2 - Y^2)\hat{\mathbf{x}}, (X^2 - Y^2)\hat{\mathbf{y}}$
T_4	XY	\mathbf{T}_5'	$XY\hat{\mathbf{x}}, XY\hat{\mathbf{y}}$
T_5	iX, iY	$\mathbf{T}_1 + \mathbf{T}_2 + \mathbf{T}_3 + \mathbf{T}_4 :$	
		\mathbf{T}_1	$\frac{i}{\sqrt{2}}(X\hat{\mathbf{x}} + Y\hat{\mathbf{y}})$
		\mathbf{T}_2	$\frac{i}{\sqrt{2}}(Y\hat{\mathbf{x}} - X\hat{\mathbf{y}})$
		\mathbf{T}_3	$\frac{i}{\sqrt{2}}(X\hat{\mathbf{x}} - Y\hat{\mathbf{y}})$
		\mathbf{T}_4	$\frac{i}{\sqrt{2}}(Y\hat{\mathbf{x}} + X\hat{\mathbf{y}})$